JOURNAL OF AIRCRAFT
Vol. 45, No. 4, July–August 2008

Boundary-Layer Control by Hydrophilic Surfaces

Daniel Favier* and Christian Maresca†
Centre National de la Recherche Scientifique, 13009 Marseille, France
Wolfgang Geissler‡
Institute of Aerodynamic and Flow Technology, Goettingen, 37073, Germany
and
Marcellin Nsi Mba§ and Patrick Sainton¶
Centre National de la Recherche Scientifique, 13009 Marseille, France

DOI: 10.2514/1.34716

Effects due to hydrophilic surfaces are investigated on an airfoil by means of both experimental and numerical approaches. Boundary-layer velocity profiles are measured by embedded laser Doppler velocimetry along the NACA0012 airfoil upper-side surface on two identical wings (one of them being coated using hydrophilic treatment). Present experimental results clearly show that the hydrophilic treatment induces a positive viscosity gradient at the wall that significantly delays the boundary-layer separation occurrence and thus provides a favorable effect on lift-coefficient increase and drag-coefficient reduction. From solution of time-dependent Navier–Stokes equations, the numerical approach is conducted by accounting for the modification of the surface boundary condition as a slip-velocity condition. Different values of the slip velocity are investigated and compared with the reference case of a no-slip boundary condition. Calculated lift-and-drag coefficients well confirm the improvement due to a velocity slip along the airfoil boundary. The calculation results also show that the slope of velocity profiles at the airfoil surface is increased due to slip and that separation has partly or totally been avoided. Finally, the present experimental and numerical results indicate that aerodynamic benefits are clearly provided by hydrophilic surface treatments.

Nomenclature

a	=	sonic flow velocity, m s^{-1}
C, c	=	airfoil chord, m
C_D	=	drag coefficient
C_f	=	skin-friction coefficient at the wall
C_L	=	lift coefficient
C_p	=	pressure coefficient at the wall
F	=	frequency of jet pulses, Hz
M	=	Mach number, U_∞/a
N	=	number of oscillation cycles of the jet per dynamic stall period
$\mathbf{n}$	=	normal at the wall
Re	=	Reynolds number, $U_\infty c/\nu$
S	=	curvilinear X coordinate, m
U	=	streamwise component of the velocity, m s^{-1}
U_s	=	constant slip velocity, m s^{-1}
U_∞	=	wind-tunnel velocity, m s^{-1}
V	=	normal component of the velocity, m s^{-1}
V_T	=	velocity of the running-belt slip, m s^{-1}
V_0	=	steady part of the blowing velocity $(V_0 + V_1 \sin(N\omega^* T))$, m s^{-1}
V_1	=	amplitude of the oscillatory part, $(V_0 + V_1 \sin(N\omega^* T))$, m s^{-1}
X, x	=	streamwise coordinate, m
Y, y	=	normal distance to the wall, m
α	=	airfoil incidence angle, deg
α_{jet}	=	jet inclination angle, deg
ν	=	kinematic viscosity, m^2 s^{-1}
ρ	=	fluid density, kg/m^{-3}
ω^*	=	reduced frequency of jet pulses, $2\pi f c/U_\infty$

Received 26 September 2007; revision received 27 February 2008; accepted for publication 29 February 2008.

*Senior Research Scientist, Director, Laboratoire d'Aérodynamique et de Biomécanique Du Mouvement, Université de la Méditerranée 163, Avenue de Luminy, Boite Postale 918; daniel.favier@univmed.fr. Senior Member AIAA.

†Senior Research Scientist, Laboratoire d'Aérodynamique et de Biomécanique Du Mouvement, Université de la Méditerranée 163, Avenue de Luminy, Boite Postale 918; christian.maresca@univmed.fr. Associate Fellow AIAA.

‡Senior Research Scientist, Bunsenstrasse 10; wolfgang.geissler@dlr.de.

§Research Engineer, Laboratoire d'Aérodynamique et de Biomécanique Du Mouvement, Université de la Méditerranée 163, Avenue de Luminy, Boite Postale 918; nsi-mba@univmed.fr.

¶Study Engineer, Laboratoire d'Aérodynamique et de Biomécanique Du Mouvement, Université de la Méditerranée 163, Avenue de Luminy, Boite Postale 918; patrick.sainton@univmed.fr.

I. Introduction

A LITERATURE survey indicates that numerous methods of flow control have already been successfully used with practical engineering devices [1]. The control is shown to be closely linked to physical phenomena originating from the boundary-layer flow and its behavior. Thus, delaying transition from laminar to turbulent flow, preventing separation, and reducing the skin-friction drag are the more common strategies generally used in active and passive control [2–5].

The skin-friction drag reduction can be obtained through methods involving geometries introduced in the surrounding of the surface, such as those described in [6,7]. Some other methods used to reduce the skin-friction drag involve a foreign substance (large-length-to-diameter particles, spherical particles, macrofibers, and polymers). Such substances are introduced within the main flow at very low concentration and are transferring a non-Newtonian behavior to the flow [8].

More recently, a reactive control was realized by painting the surface with a substance reacting with the surrounding fluid. A typical example is given by hydrophilic surfaces [9–12]. In this case, the reaction between the wet flow and the deposit also results in a significant drag reduction. This reducing effect has already been observed with skiers [13] and boat and car drag [11]. Briefly, it can be stated that the wetter the surrounding fluid is, the more efficient the drag-reduction effect will be.

Another way to reduce the skin friction at the wall of a body is to introduce a suction process at the surface to possibly prevent the

boundary-layer separation [14]. The mechanism of drag reduction and of separation prevention were observed in reactive control using hydrophilic surfaces, where the phenomena of wall suction and gradient of viscosity are present and can be understood from the following considerations. In 1904, Prandtl gave the first explanation of the mechanism of boundary-layer separation over a fixed wall in the case of steady and two-dimensional flow. He provided a criterion for the point of separation at the wall:

$$u|_{y=0} = 0; \qquad \left.\frac{\partial u}{\partial y}\right|_{y=0} = 0 \tag{1}$$

Behind this separation point, fluid particles close to the wall move against the external fluid (separated flow). That means that the velocity profile must have an inflexion point somewhere above the wall. It is well known that the condition $(\partial^2 u/\partial^2 y)_{y=0} > 0$ is necessary for the separation of a two-dimensional steady boundary layer. However, a negative curvature of the velocity profile at the wall must be a sufficient condition for the flow to remain attached. It becomes clear that the boundary-layer control (advancing or delaying the separation) could be closely linked to the shape of the velocity profile near the wall. One of the best ways to control the separation delay is then to keep the term $(\partial^2 u/\partial y^2)_{y=0}$ as negative as possible or to make the velocity profile as full as possible. From the streamwise momentum equation written at the wall [1],

$$\rho \nu_w \left.\frac{\partial u}{\partial y}\right|_{y=0} + \left.\frac{\partial p}{\partial x}\right|_{y=0} - \left.\frac{\partial \mu}{\partial y}\right|_{y=0} \left.\frac{\partial u}{\partial y}\right|_{y=0} = \mu \left.\frac{\partial^2 u}{\partial y^2}\right|_{y=0} \tag{2}$$

it can be deduced that the separation control methods will use different ways to keep $(\partial^2 u/\partial y^2)_{y=0}$ as negative as possible:

1) Maintain a vertical velocity at the wall: $\nu_w < 0$; that is, maintain a wall suction.

2) Maintain a favorable pressure gradient: $\partial p/\partial x|_{y=0} < 0$.

3) Realize a lower viscosity of the fluid at the wall: $\partial \mu/\partial y|_{y=0} > 0$.

A particular case of wall suction can be realized by introducing a wall tangential velocity, as provided by a belt moving at the wall in the same direction as the main stream. This case will be specifically considered in the numerical part of the present paper. It will be shown that the main effect of a wall velocity consists of providing the separation delay, as clearly demonstrated by the velocity profiles obtained numerically.

When examining the preceding item 3, fluids generally used in experiments relative to boundary-layer control are physically homogenous (i.e., $\partial \mu/\partial y = 0$). It is well known that non-Newtonian fluids such as polymer solutions [8] may help to control the wall separation by an effect of viscosity acting on the shape of the velocity profile at the wall; nevertheless, $\partial \mu/\partial y$ remains equal to zero at the wall. But the situation in which the fluid is less viscous at the wall than in the main flow, as is the case for hydrophilic surfaces [9–12], can also be realized, as will be shown in the experimental part of the present paper. Moreover, it is also possible that the surface may extract water particles from the near flow in this case, resulting in a thin film of water at the surface. This film may act as a lubricant for the surrounding airflow, and it is assumed that the interface between the water film and the airflow is moving downstream at a constant velocity. Although no viscosity gradient at the wall can be numerically taken into account in the present numerical approach, the water-film phenomenon has nevertheless been simulated by introducing into the code a virtual slip velocity at the wall. It was shown here that such a condition is equivalent to a particular case of wall suction, favorable to a separation delay.

The effect of $\partial \mu/\partial y > 0$ at the wall associated with the formation of a thin water film at the surface creates favorable effects on the delay of the boundary layer. This will be explained in detail by the velocity profiles and overall forces shown in the experimental part of the paper (Sec. II). The numerical investigation (Sec. III) will well confirm that a virtual slip wall velocity, as supposed, will delay the boundary-layer separation, as will be shown on the velocity profiles and overall forces calculated.

II. Experimental Investigation

Hydrophilic surface treatments have been recently applied to engineering and sport devices to successfully reduce the drag skin friction. A few examples can be found [13,15] for skis, bobsleigh skates, boat and car shells, the internal surface of rubber gloves, etc. The kind of surface treatment proposed in this study consists of the following processes [9]: 1) abrasion of the surface in the length direction, 2) thermal treatment with a superficial air jet at 102–125°C during 1 min, and 3) fixation of a hydrophilic coat by use of a woolly rotary brush.

The present experimental investigation thus aims to apply the hydrophilic process to an airfoil set at high incidence in the wet airflow of a wind tunnel. The objective is specifically to prove the benefic effect of such a treatment surface on the drag reduction at the wall and, in particular, to see if the separation occurrence can be avoided. Overall forces (lift and drag) and boundary-layer velocity-profile measurements will be efficient to prove the wall friction reduction and the separation delay.

The investigation was carried out on two identical wings of a symmetrical NACA0012 airfoil. Before the surface treatment, the two wings had strictly the same external geometries (planform, airfoil profile, dimension, surface roughness, etc.) and identical aerodynamic behaviors regarding the lift, drag, and moment coefficient variations as a function of the airfoil angle of attack, ranging up to the high values that generate the static stall and poststall conditions. One of the wings then received the hydrophilic coating treatment, as described. The two wings (coated and uncoated) were then tested in the same 2-D airflow at the same low Reynolds number ($Re \approx 10^5$) and same angles of attack of the airfoil (closer and higher than the static stall incidence). Measurements of the velocity components through the boundary layer were measured in different streamwise stations, ranging from the leading to the trailing edge and using an embedded laser Doppler velocimeter (ELDV) 3-D system [16–19]. Overall forces, measured by help of a balance [17], and velocity profiles obtained on the two wings in the same experimental conditions were then compared to characterize the effect of the hydrophilic treatment.

A. Experimental Apparatus

The experiments were conducted in the open-circuit S2L wind tunnel of the Laboratoire d'Aérodynamique et de Biomécanique Du Mouvement (LABM). The freestream velocity U_∞ in the rectangular test section (1×0.5 m with a length of 3 m) can be varied from 2 to 20 m s^{-1} with a natural turbulence rate lower than 0.5%. Each wing (0.3 m in chord and 0.495 m in height) vertically mounted between the walls of the wind tunnel was equipped with the ELDV system operating in a 2-D-component configuration, as shown in Fig. 1.

As sketched in Fig. 2, velocity profiles are measured by use of a 2-D ELDV system. The optical components of the velocimeter (focal head and beam expander) operating in the back scattering mode are gathered on a platform located beneath the floor of the wind tunnel. The survey of the velocity vector along the local normal to the surface is carried out using a displacement-controlled system of the optical head of the velocimeter [16–18]. The measurement volume is formed by crossing the two volumes provided by the green ray (wavelength $\lambda = 514.5$ nm, length $dz = 6.08$ mm, width $dy = 0.24$ mm, height $dx = 0.24$ mm, and fringe $i = 6.44$ mm) and the blue ray (wavelength $\lambda = 488.0$ nm, length $dz = 5.75$ mm, width $dy = 0.23$ mm, height $dx = 0.23$ mm, and fringe $i = 6.10$ mm). This measurement volume can be displaced normally to the wall from $y = 0.2$ to 200 mm by steps of 0.1 mm, with an accuracy measurement less than 0.05 mm. The streamwise displacement of the probe along the normal to the wall is allowed for all abscissa ranging from the leading to the trailing edge [16].

On the two wings, data bursts delivered by the measuring volume are successively gathered through two burst spectrum analyzers and finally transmitted toward a computer PC data treatment. The calculation is done by software developed at LABM under the symbolic-language LabVIEW system [16–18]. At a fixed streamwise coordinate $x/C =$ constant (Fig. 3) and for a given altitude y

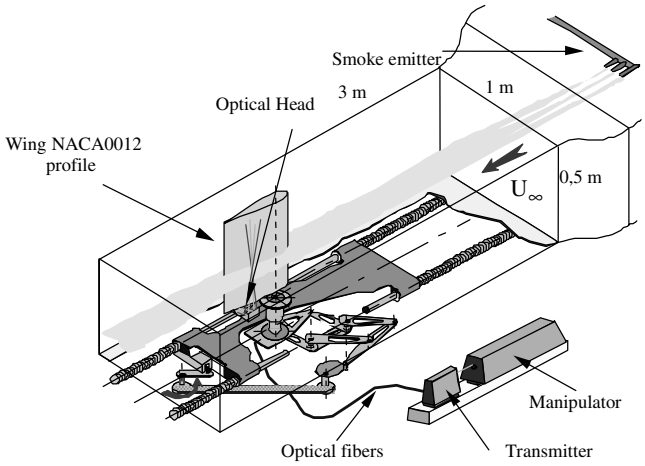

Fig. 1 Experimental apparatus.

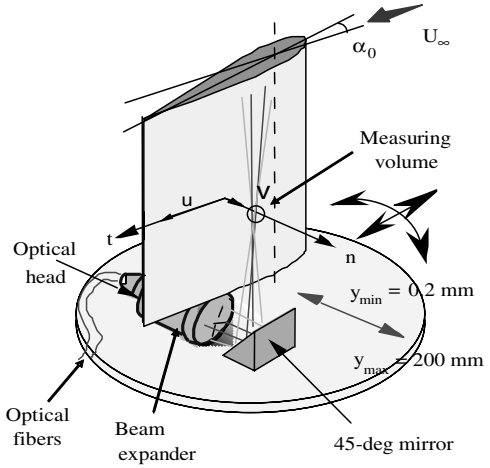

Fig. 2 ELDV system.

above the wall, measurements carried out by ELDV provided the two velocity components (u, v) that are submitted to the following acquisition and treatment procedures.

For each velocity component (u streamwise, v normal), the acquisition relative to a couple of parameters ($x =$ constant and $y =$ constant) concerns the recording of doublets (time and velocity) tu and tv, validated by the spectrum analyzers of the ELDV and the velocity values corresponding u or v. A number $N1$ of elementary blocks built with the four values (tu, u) and (tv, v) are thus associated with a couple of parameters (x, y). The $N1$ number of elementary blocks is generally fixed to 100 blocks of 512 values: that is, a total number $N = 51,200$ of elementary doublets (tu, u) and (tv, v). A statistical average is then performed on 51,200 values of u and v. The average values are noted U and V. About 30 altitudes are thus surveyed on a local normal of the airfoil to define a velocity profile. Using the aforementioned data-reduction procedure and the high N number of elementary doublets, the relative accuracy of ELDV measurements is shown to be less than 1% on the U component and less than 2% on the V component, as far as unseparated flow conditions are concerned. When flow conditions involve the boundary-layer separation, the relative accuracy measurement is increased to 2% on the U component and to about 4% on the V component [16–18].

An embedded three-component balance is additionally used to measure the aerodynamic instantaneous efforts (lift, drag, and pitching moment) experimented by the wing. The relative accuracy measurement is less than 0.5% on the lift force, less than 1% on the drag force, and about 1.5% on the airfoil pitching moment [17].

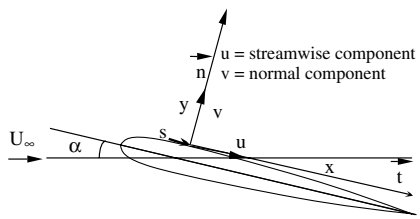

Fig. 3 Boundary-layer reference axis system.

B. Experimental Results

1. *Velocity Profiles Obtained on the Uncoated Wing*

Velocity components u and v were measured on the two wings at different stations x/c located between $x/c = 0.05$ and 0.70 for y varying from $y = 0.20$ to 50 mm and $U_\infty = 5\ \mathrm{m\,s^{-1}}$. Elementary samples on u and v were averaged from 100 blocks of 512 values, according to the preceding method. As an example, for an airfoil incidence of $\alpha = 13$ deg, Fig. 4 gives two profiles of the streamwise velocity U obtained at $x/c = 0.05$ and 0.23 in the case of the uncoated wing.

Velocity-profile behavior (Fig. 4, left) was typically that of an attached boundary layer at the leading edge. Further downstream along the airfoil chord (Fig. 4, right), negative values were obtained for U at $y < 4$ mm, indicating the occurrence of the boundary-layer separation. The increase of the velocity in the external flow compared with the value of the airflow of the wind tunnel was due to the pressure gradient along the airfoil's upper side. Figure 5 also illustrates the capability of such boundary profiles to accurately characterize the boundary-layer behavior.

The streamwise location of the measurement volume was set at $x/c = 0.19$, and the airfoil incidence angle varied discretely from 12 (below the static stall incidence) to 14 deg. An increase of the boundary-layer thickness with the airfoil incidence angle can be noticed, as expected, resulting in a reverse flow ($U < 0$) at incidence values higher than the stall incidence.

Figure 6 presents the evolution of the U streamwise component from $x/c = 0.050$ to 0.272 at the stall incidence of $\alpha = 13$ deg. This expected behavior of the boundary-layer thickening from the leading to trailing edge is clearly pointed out by the successive velocity profiles, confirming that the boundary layer is well separated, at least over the whole upper-side airfoil region surveyed.

2. *Velocity Profiles Obtained on the Coated Wing*

Velocity-profile measurements were performed in the same way at the stalled incidence $\alpha = 13$ deg and for $0.05 \le x/c \le 0.70$. The analysis of the influence of the surface treatment was carried out by comparison between the U streamwise-component velocity obtained on the two wings. Figures 7a–7c present a comparison of the U component obtained successively on the untreated and treated surface wings. It can be seen that in the case of the untreated wing, the reverse flow (separation of boundary layer) occurs at $x/c = 0.19$ (Fig. 7a) with a strong thickening of the boundary layer. It is worth noting that at the same x/c value, the U streamwise component remains positive on the coated wing (Fig. 7b), meaning clearly that the boundary layer is attached at this station and remains in such an attached configuration at least back to $x/c = 0.70$ (Fig. 7c).

A direct consequence of the wing surface treatment was to keep the boundary layer attached at higher incidence (higher than the static stall value) over a large part of the upper side of the airfoil. It can be concluded from the analysis of the experimental profiles developed through the boundary layer on the upper side of the airfoil's coated wing that the hydrophilic treatment delays the stall process. This treatment acts like a reattachment device of the boundary layer. It will be shown in the numerical part of the present study that the same effect can be also obtained by introducing a wall-component velocity in the Navier–Stokes equations.

3. *Comparison of Overall Forces Acting on the Two Wings*

Figure 8 shows the variation with airfoil incidence of lift C_L and drag C_D coefficients obtained on the two wings using the balance

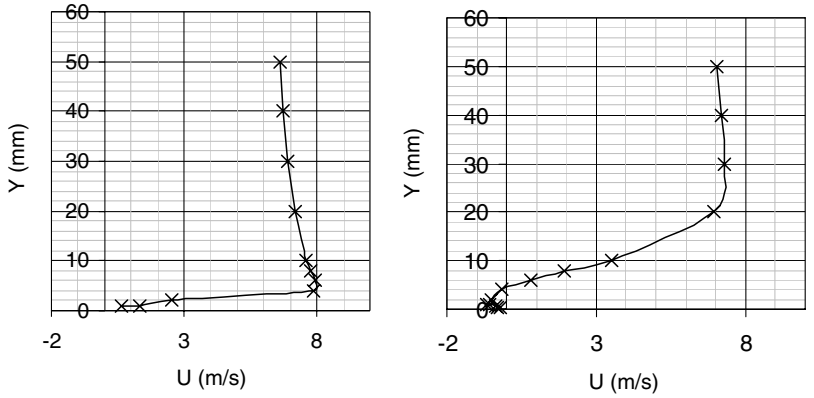

Fig. 4 Streamwise velocity component $U = f(y)$ at $\alpha = 13$ deg: $x/c = 0.05$ (left) and $x/c = 0.23$ (right).

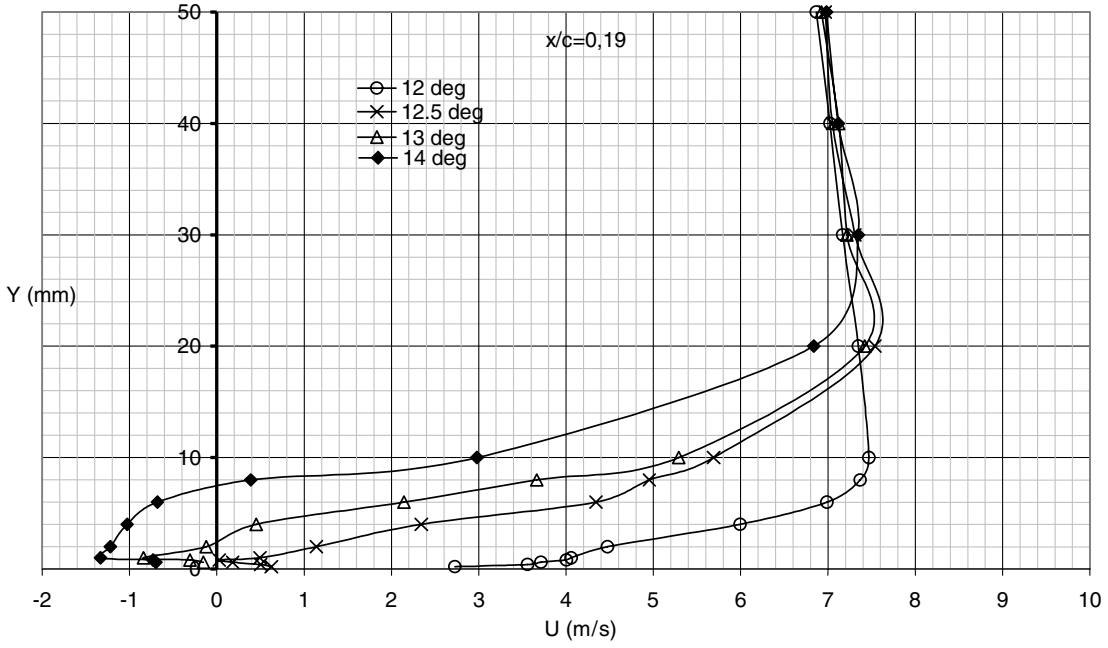

Fig. 5 Variation of $U = f(y)$ with the airfoil incidence.

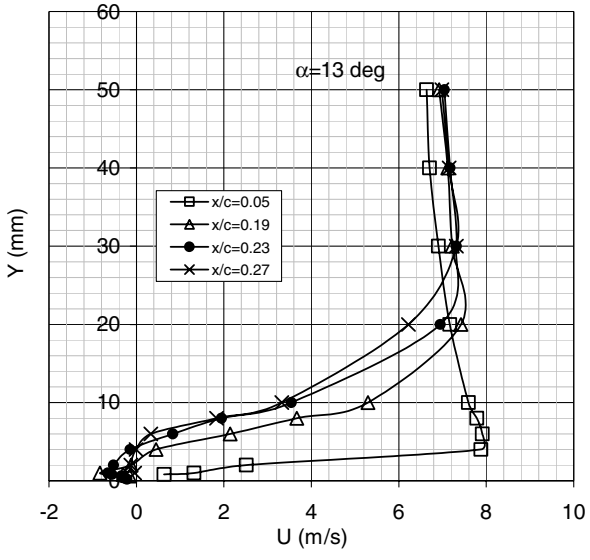

Fig. 6 Streamwise variation of $U = f(y)$ at $\alpha = 13$ deg.

measurement described. The maximum lift is shown to be obtained in the two cases at quite the same airfoil incidence angle of $\alpha = 11.75$–12 deg. The delay of separation over 70% of the upper side of the airfoil's coated wing observed on the velocity profiles induces a higher lift force, particularly when the static stall angle is overlapped. At the static stall incidence value, the gain on lift due to the hydrophilic upper-side surface is about 8%, and that on drag reduction is evaluated at about 3%. It must be noticed that such gains would have been higher if the whole airfoil surface (upper and lower sides) had been treated.

III. Numerical Investigation

For the numerical simulation of a hydrophilic upper-side airfoil surface, it is assumed that the boundary condition along the modified surface is changed from the usual no-slip boundary condition to a slip boundary condition associated with a positive gradient of viscosity at the wall. In the last case, the velocity along the treated surface has a finite and prescribed value. For the present study, the amount of slip velocity is not known and the numerical code is not available for simulating a viscosity gradient at the wall. Only a systematic parametric study with variable prescribed slip velocities can deliver the necessary information about the effect obtained on velocity

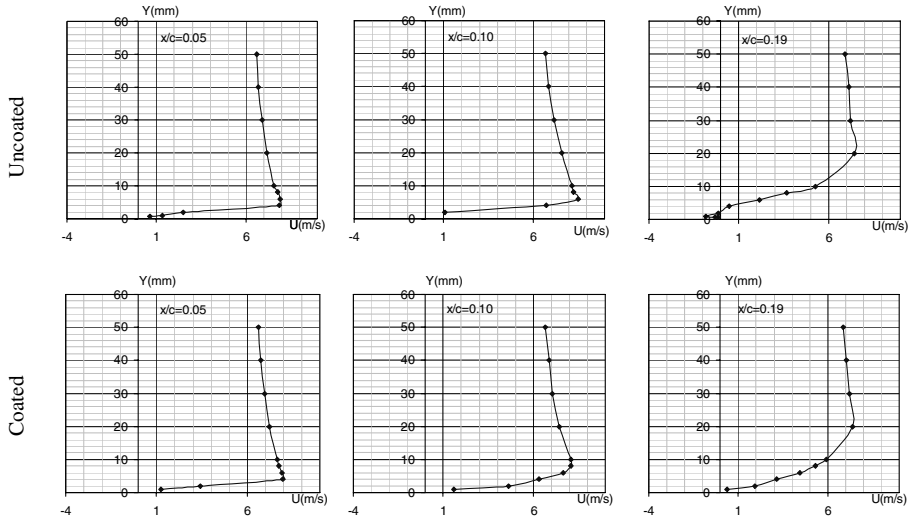

a) Streamwise velocity component U=f(y) on coated/uncoated surface : 0.05<x/c<0.19

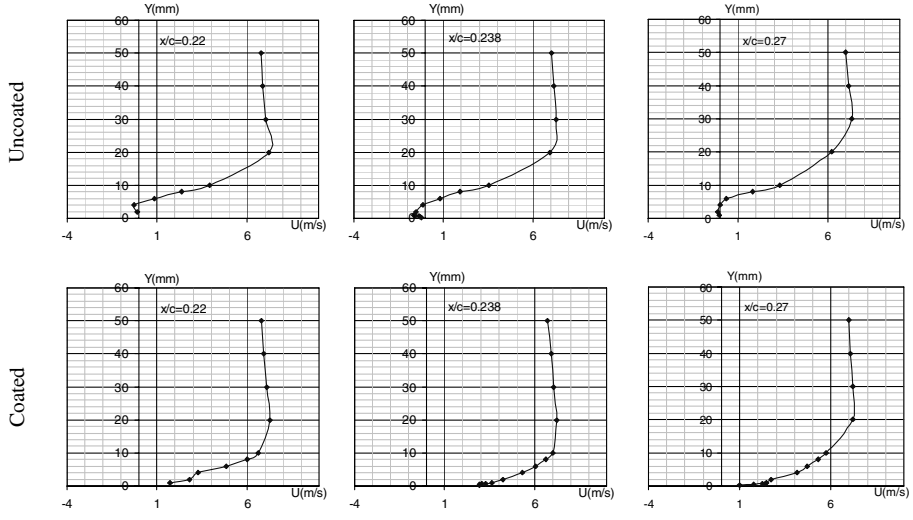

b) Streamwise velocity component U=f(y) on coated/uncoated surface : 0.22<x/c<0.27

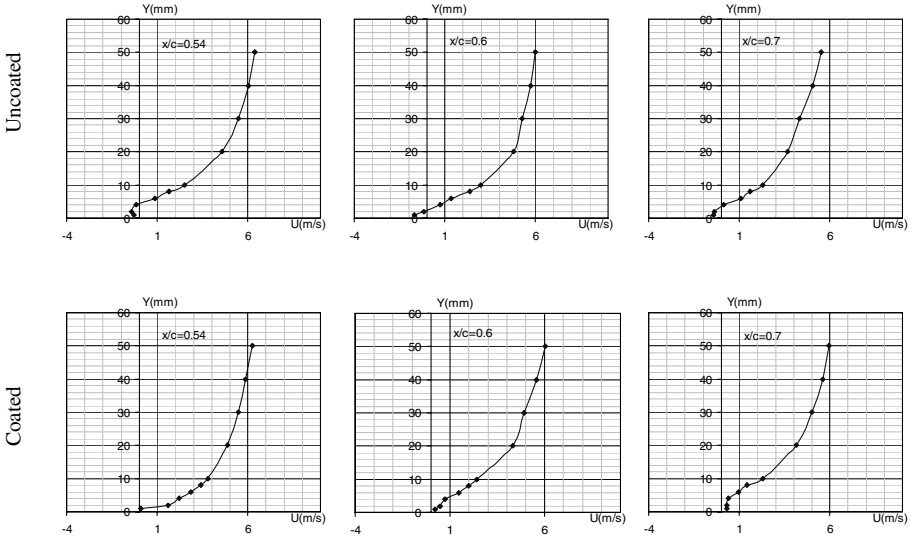

c) Streamwise velocity component U=f(y) on coated/uncoated surface : 0.54<x/c<0.70

Fig. 7 Streamwise velocity component $U = f(y)$ on coated/uncoated surface: a) $0.05 < x/c < 0.19$, b) $0.22 < x/c < 0.27$, and c) $0.54 < x/c < 0.70$.

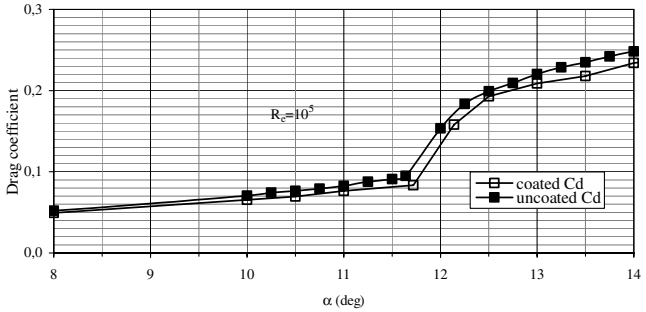

a) Comparison of drag coefficient on coated and uncoated wings

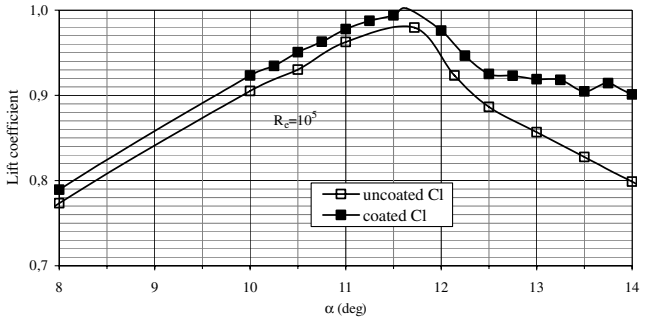

b) Comparison of lift coefficient on coated and uncoated wings

Fig. 8 Comparison of coefficients on coated and uncoated wings.

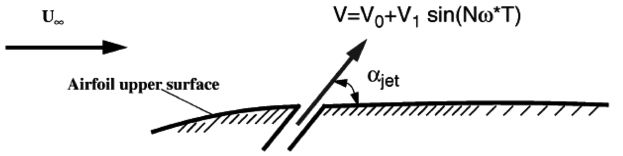

Fig. 9 Family of surface boundary conditions.

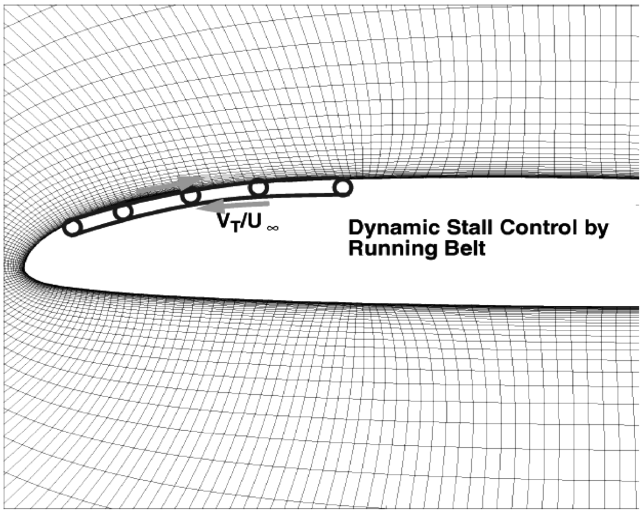

Fig. 10 Running-belt concept.

profiles in the boundary layer and on pressures and forces acting on the airfoil surface. These results are then compared with data obtained from calculations with no-slip condition and, finally, with data measured with both untreated and treated airfoil surfaces in Sec. II.

A. Numerical Code

For the present calculations, a 2-D time-accurate Navier–Stokes code [19] was used. This code is based on the approximate factorization implicit methodology, originally developed by Beam and Warming [20]. The code has already successfully been applied for a number of investigations [21,22] to calculate dynamic stall and dynamic stall control problems on oscillating airfoils of helicopter rotors and wind-energy converters. Different turbulence and transition models are available in this code. A comprehensive discussion of turbulence modeling for aeronautical application can be found in [23]. In the present study, the Spalart–Allmaras one-equation turbulence model [24] was used. Transition from laminar to turbulent flow is assumed to be "free transition," taking into account Michel's criterion [25], to determine transition onset and applies exponential growth from laminar to fully turbulent flow, as described in [26]. Previous simulations have shown that the numerical accuracy is generally less than 0.1% for lift force prediction and a little bit higher for local flow quantities (less than 0.2% for the streamwise U component) [21,22].

B. Family of Boundary Conditions

The numerical code has recently been modified to apply a family of boundary conditions for the investigation of flow control problems. Figure 9 shows the introduction of modified boundary conditions for application of the synthetic jet concept to control dynamic stall. In this special case, velocity pulses are introduced from a very narrow gap on the airfoil surface. The prescribed velocity pulses have a constant (i.e., time-independent) term V_o and the amplitude of an unsteady sinusoidal term V_1, allowing both suction and blowing with a prescribed frequency $N\omega^*$ (reduced frequency $\omega^* = 2\pi fc/U_\infty$). The velocity pulses $V_0 + V_1 \sin(N\omega^* T)$ may be directed along a prescribed angle α_{jet} measured against the surface slope (see Fig. 9). In the present case, a constant slip velocity is assumed along the upper surface of the airfoil. In this special case, the unsteady part V_1 of the prescribed velocity is set equal to zero. The steady part V_0 is assumed to be constant along the treated part of the surface, and the inclination angle α_{jet} is also set equal to zero.

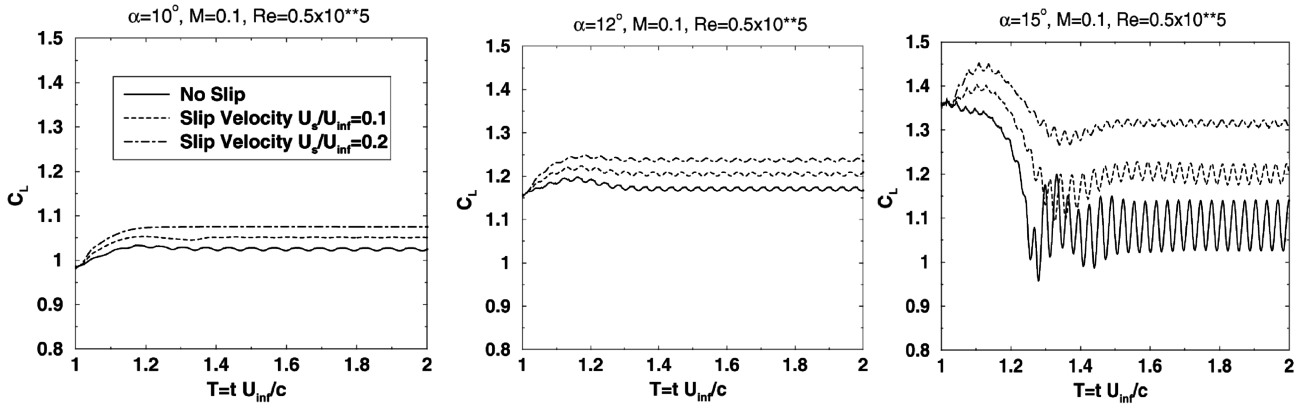

Fig. 11 Time-dependent lift distributions.

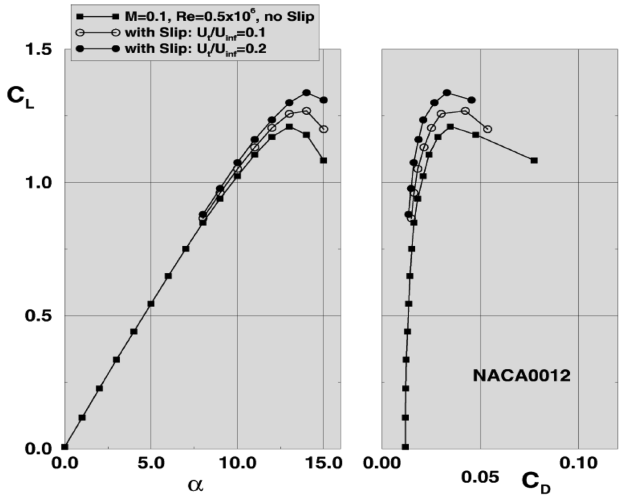

Fig. 12 Lift-and-drag polar with and without slip.

Figure 10 shows a possible application of this special case to simulate a constant slip velocity along a prescribed airfoil surface. Assuming that a piece of surface is replaced by a "running belt" that is moving with a permanent and constant velocity V_T. By placing the belt at the right position, it has been shown that a considerable benefit is achieved to improve dynamic stall properties. In this case, the velocity ratio V_T/U_∞ has to be rather high (about unity) for optimal control. In the present investigation, the surface is covered by a hydrophilic material. In this case, it is assumed that the slip velocities are rather small. Three cases will be investigated: 1) no-slip condition, 2) slip with $U_s/U_\infty = 0.1$, and 3) slip with $U_s/U_\infty = 0.2$

Velocity U_s is representing the corresponding constant slip velocity along the prescribed (i.e., treated) part of the airfoil surface. This active part of the surface is the complete upper surface of the airfoil, as realized in the experiments. All cases will be investigated for the incidence regime 0 deg $<\alpha <$ 15 deg (no slip) and 8 deg $<\alpha <$ 15 deg (with slip). The present numerical code is a compressible code. A reduction of the Mach number beyond $M = 0.1$ may therefore cause some problems. Therefore, all calculations were carried out with $M = 0.1$ and $Re = 0.5 \times 10^6$. It is obvious that the slightly higher Mach and Reynolds numbers compared with measurements will not allow a direct comparison of the results. Only trends of both calculation and experiment are thus comparable.

C. Results

The numerical calculations were carried out in time-accurate mode. From steady starting conditions obtained with the no-slip boundary condition, calculations are continued in a dimensionless time frame: $1 < T < 2$ with $T = tU_\infty/c$. As many as 10^5 time steps per case were used. The time-dependent lift results in Fig. 11 show that the number of time steps and the chosen time frame are sufficient to reach cyclic converged on constant values.

1. *Lift-and-Drag Polars*

Figure 11 shows lift distributions versus dimensionless time T for the three cases of no slip and slip with $U_s/U_\infty = 0.1/0.2$. In all cases, lift is remarkably increased with increasing slip velocity. In most cases, a time dependency is observed that is considerably larger in the case of $\alpha = 15$ deg (Fig. 11, right). It is of interest that the amplitudes of oscillations are reduced with increasing slip velocity.

Figure 12 shows lift-and-drag polars for the three cases investigated. These results are based on the average values of Fig. 11. It is clearly demonstrated that with increasing slip velocity, lift is

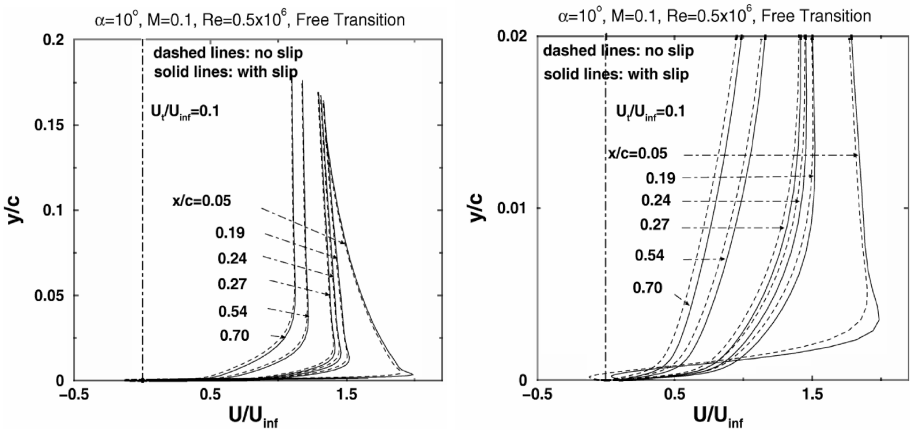

Fig. 13 Velocity profiles at selected positions of the upper surface: global view (left) and focused view close to the surface (right).

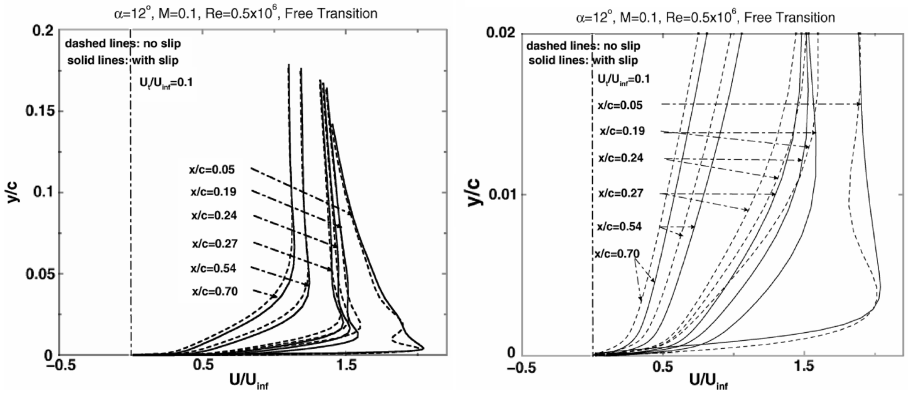

Fig. 14 Velocity profiles at selected positions x/c of the upper surface: global view (left) and focused view close to the surface (right).

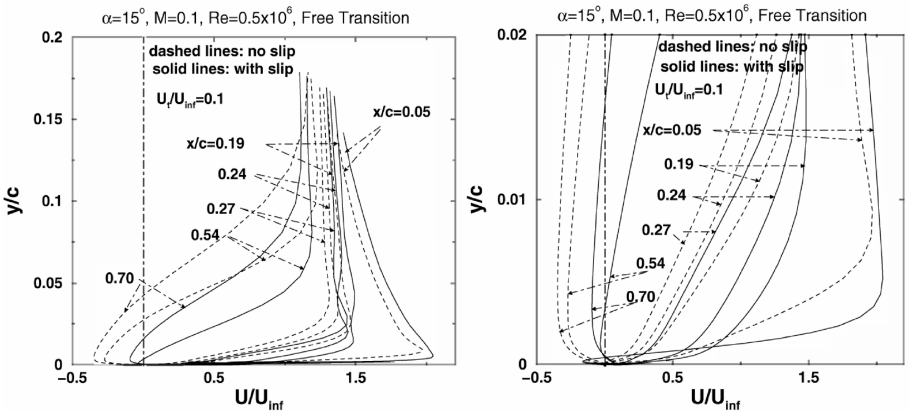

Fig. 15 Velocity profiles at selected positions x/c of the upper surface: global view (left) and focused view close to the surface (right).

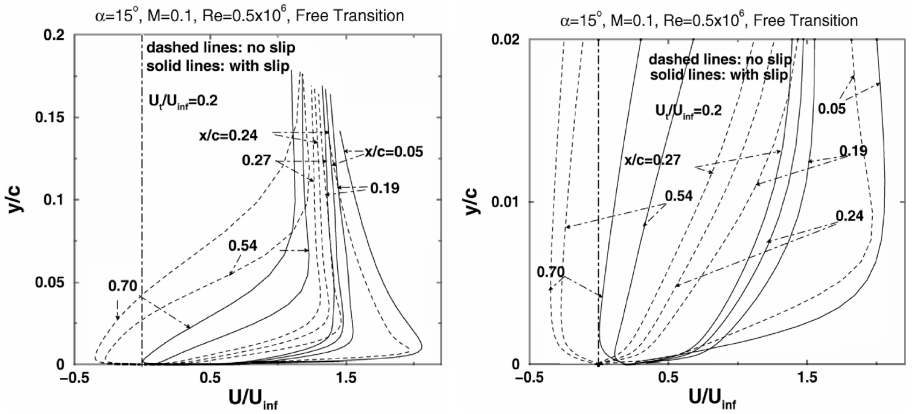

Fig. 16 Velocity profiles at selected positions x/c of the upper surface: global view (left) and focused view close to the surface (right).

considerably increased to rather high maximum lift values. At the same time, drag is reduced with increasing slip. These general results are in good qualitative comparison with the experimental data shown in the previous section.

2. Flow Details

Lift-and-drag forces show improvements due to surface slip. To better understand the effects of finite slip velocities along the surface, it is necessary to have a look into the flow details (i.e., to study the development of boundary-layer profiles with and without slip). These data may then be directly compared with ELDV measurements. Figures 13–15 show velocity profiles at six positions x/c along the upper surface of the airfoil. The cases of the no-slip condition (dashed lines) are compared with results obtained with slip: $U_s/U_\infty = 0.1$ (solid lines). The two lower incidences $\alpha = 10$ and 12 deg (Figs. 13 and 14) do not show a severe separation, except a very narrow separation bubble at 5% chord in Fig. 14. In these incidence cases, the slope of the velocity profiles at the airfoil surface is increased with slip, compared with the no-slip cases.

Increased effects are seen at the highest incidence $\alpha = 15$ deg in Fig. 15, in which a severe separation occurs over large parts of the upper surface of the airfoil. Introducing slip, separation is either reduced or was completely avoided. An exception occurs at $x/c = 0.05$ (Fig. 15, right), where a narrow separation bubble develops for the case with slip. This bubble disappears with a higher slip velocity ($U_s/U_\infty = 0.2$), displayed in Fig. 16 for the same incidence case $\alpha = 15$ deg. It has to be pointed out that the different velocity profiles are time-averaged (see Fig. 11).

From numerical calculations, the surface pressure and skin-friction distributions are also available. Figure 17 shows examples of both C_p and C_f distributions versus airfoil chord at $\alpha = 15$ deg for the two cases of no slip and slip with $U_s/U_\infty = 0.1$. With slip, the pressure distribution on the upper surface exceeds the values, and no slip causes increased lift. The skin-friction distribution shows increased (positive) values over the forward portion of the airfoil. Further downstream, the C_f values are mostly less negative than with the no-slip case. At the airfoil leading edge, a small separation bubble develops in both cases. The transition from laminar to turbulent flow takes place over this bubble, as can be observed in Fig. 18, in which the calculated transition region is shown for the no-slip case (left), the slip case $U_s/U_\infty = 0.1$ (middle), and the slip case $U_s/U_\infty = 0.2$ (right).

The time dependency of the results, as already indicated in Fig. 11, is also visible in Fig. 18. In the no-slip case, the transition is moving

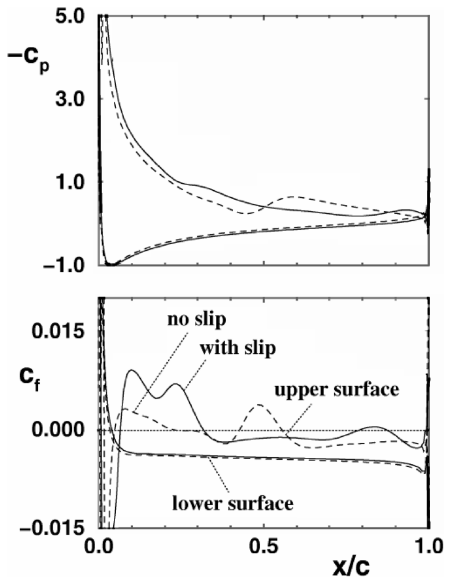

Fig. 17 Pressure and skin-friction distributions versus chord; $a = 15$ deg.

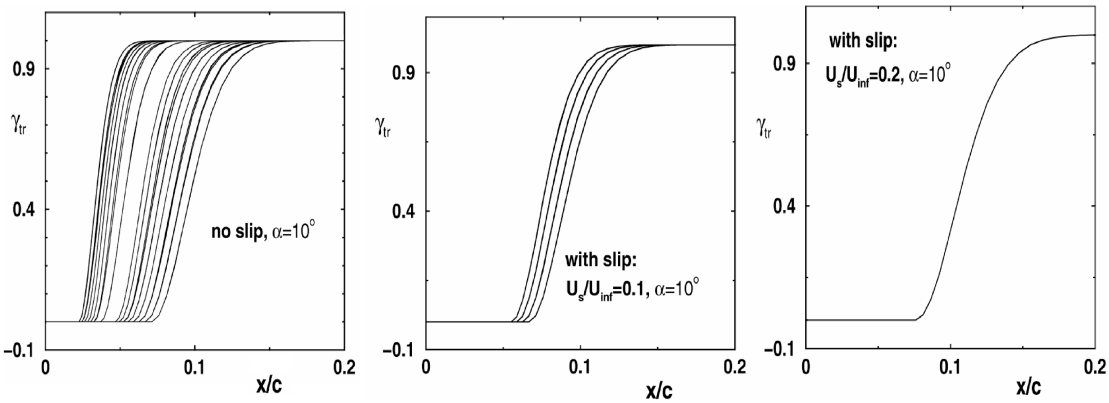

Fig. 18 Transition locations on upper surface.

several percent of the airfoil leading edge, representing a time-dependent transition zone. With a small slip velocity ($U_s/U_\infty = 0.1$), this region is considerably reduced. A further increase of slip velocity ($U_s/U_\infty = 0.2$) finally leads to a single transition curve, corresponding to the time-independent lift (see Fig. 11). For higher incidences, similar effects were detected. At $\alpha = 15$ deg, the time dependency is always present. The amplitudes of oscillation of the transition regime are reduced with increasing slip velocity.

IV. Conclusions

The paper aimed to explain the drag-reduction phenomenon observed when using hydrophilic surfaces. Momentum equations show that a positive viscosity gradient at the wall and/or a slip wall velocity are among the favorable factors of this drag-reduction effect.

The experimental results obtained on the 2-D velocity profiles inside the boundary layer developed over two wings (one of them is hydrophilic) set at high incidence and low Reynolds number in the stream of a wind tunnel clearly showed that the main effect of the hydrophilic treatment was to significantly delay the boundary-layer separation. This effect was confirmed by the measured lift and drag. At the static stall incidence value, the gain on lift due to the hydrophilic upper-side surface was about 8% and that on drag reduction was evaluated at about 3%.

On the other hand, numerical calculations on the basis of the solution of the time-dependent Navier–Stokes equations were carried out, taking into account the modification of the surface boundary condition as a slip condition. Two different slip velocities, $U_s/U_\infty = 0.1$ and 0.2, were investigated and compared with the reference case of a no-slip boundary condition. The treated part of the airfoil is the complete upper surface of the airfoil, as was also realized in the experiments. Calculated lift-and-drag polars show considerable improvements due to a velocity slip along the airfoil boundary. The maximum lift is increased as much as 5% ($U_s/U_\infty = 0.1$) and 10% ($U_s/U_\infty = 0.2$).

The numerical results also show that the slope of velocity profiles at the airfoil surface is increased due to slip and that separation has partly or totally been avoided. In the regime of flow separation, increased unsteadiness was calculated. With increasing slip velocity, the amplitudes of lift oscillations are strongly reduced. Although it has not been possible to directly compare experimental and numerical data sets, it can be concluded, however, that the same effects due to the hydrophilic treatment on the wing were confirmed by the two ways of investigation. Although much work remains to be done in the domain, the present experimental and numerical approaches clearly showed the aerodynamic benefits provided by hydrophilic surface treatments.

Acknowledgements

The authors gratefully acknowledge the French National Center for Scientific Research (CNRS) for the financial support provided by the Laboratoire d'Aérodynamique et de Biomécanique Du Mouvement (LABM), with Wolfgang Geissler as an Associated Senior Research Scientist. The authors also thank their colleague Alain Midol (University of Lyon I) for his kind collaboration in the surface treatment process.

References

[1] Gad El Hak, M., *Flow Control Passive, Active and Reactive Flow Management*, Cambridge Univ. Press, Cambridge, England, U.K., 2000, Chap. 8, p. 161.

[2] Buschell, D. M., "Applications and Suggested Directions of Transition Research," *Fourth Symposium on Numerical and Physical Aspects of Aerodynamic Flow*, Univ. of Southern California, Los Angeles, Los Angeles, 16–19 Jan. 1983.

[3] Huang, L. S., Maestrello, L., and Bryant, T. D., "Separation Control over an Airfoil at High Angles of Attack by Sound Emanating from the Surface," AIAA Paper 87-1261, 1987.

[4] Maestrollo, L., Badavi, F. F., and Noonan, K. W., "Control of the Boundary Layer Separation About an Airfoil by Active Surface Heating," AIAA Paper 88-3545, 1988.

[5] Blackwelder, R. F., "Some Notes on Drag Reduction in the Near wall Region," *In Flow Control Fundamentals and Practices* edited by M. Gad El Hak, A. Polland, and J. P. Bonnet, Springer–Verlag, Berlin, 1998, pp. 155–198.

[6] Wilkinson, S. P., *Direct Drag Measurements of Thin-Element Riblets with Suction and Blowing*, AIAA, Washington, D.C., 1988.

[7] Bushnell, D. M., and Hefner, J. N. (eds.), *Viscous Drag Reduction in Boundary Layer*, AIAA, Washington, D.C., 1990.

[8] Mc Comb, N. D., and Rabie, L. H., "Development of Local Turbulent Drag Reduction due to Non Uniform Polymer Concentration," *Physics of Fluids*, Vol. 22, 1979, pp. 183–185. doi:10.1063/1.862455

[9] Midol, A., Lanteri, P., Longeray, R., Zahouani, H., Mathia, T., Ribot, P., "Traitement Mécano Chimique de Surfaces Visant à Maîtriser le Frottement en Présence d'eau Sous ses Différents États; Surface de Glisse, Optimisation des Élément en Contact, Choix des Matériaux", *Journée Atlantech*, May 1996.

[10] Hirotaka, S., "Drag Reduction Method Using Combination of Hydrophobic and Hydrophilic Coatings," *58th Annual Meeting of the Division of Fluid Dynamics*, American Physical Society, Chicago, Nov. 2005.

[11] Min, T., and Kim, J., "Effects of Hydrophobic Surfaces on Skin Friction Drag," *Physics of Fluids*, Vol. 16, No. L55, 2004, pp. L55–L58.

[12] Yong-Sheng, Y., and Qing-Ding, W., "Experimental Study on Physical Mechanism of Drag Reduction on Hydrophobic Materials in Laminar Flow," *Chinese Physics Letters*, Vol. 23, June 2006, pp. 1634–1637. doi:10.1088/0256-307X/23/6/077

[13] Favier, D., Maresca, C., Berton, E., Agnès, A., and Pous, F., "Performance Optimization of a High Speed Ski Runner," *The Engineering of Sport*,Vol. 1, Blackwell Science, Boston, 2000, pp. 265–272.

[14] Antonia, R. A., Fulachier, L., Krishnamoorthy, L. V., Benebib, T., and Anselmet, F., "Influence of Wall Suction on the Organized Motion in a Turbulent Boundary Layer," *Journal of Fluid Mechanics*, Vol. 190, 1988, pp. 217–240. doi:10.1017/S0022112088001296

[15] Midol, A., Lanteri, P., Longeray, R., Mathia, T., "Sport et Technologie: Traitement Mécano-Chimique de Surfaces Visant à Maîtriser le Frottement en Présence d'eau Sous ses Différents États," *Colloque Les*

Sciences du Sport Entre Cultures et Techniques, Association for Sport and PE Research, Lausanne, Switzerland, Oct. 1995.

[16] Allain, C., "Contribution à l'Etude Expérimentale de la Couche Limite Soumise à une Instationnarité Forcée. Aplication aux Phénomènes de Transition et de Décollement en Ecoulement Instationnaire 2D/3D," Ph.D. Thesis, Univ. de la Méditerranée, Marseille, France, Nov. 1999.

[17] Favier, D., Maresca, C., Nsi Mba, M., Berton, E., and Agnes, A., "New Type of Embedded Laser Doppler Velocimeter (ELDV) for Measurement of Rotary Wings Boundary Layer," *Review of Scientific Instruments*, Vol. 68, No. 6, 1997, pp. 2447–2455. doi:10.1063/1.1148131

[18] Barla, C., Berton, E., Favier, D., and Maresca, C., "ELDV Boundary Layer Investigation on a Tilt-Rotor Rotating Blade," *Journal of Aircraft*, Vol. 43, No. 3, 2006, pp. 584–591. doi:10.2514/1.15983

[19] Geissler, W., "Unsteady Navier–Stokes Code for Accelerated Moving Airfoils Including Separation," DLR, German Aerospace Center, Rept. DLR-FB 92-03, Bonn, Germany, 1992 (in German).

[20] Beam, R. F., and Warming, R. F., "An Implicit Factored Scheme for the Compressible Navier–Stokes Equations," *AIAA Journal*, Vol. 16, No. 4, 1978, pp. 393–402.

[21] Geissler, W., Dietz, G., Mai, H., Bosbach, J., and Richard, H., "Dynamic Stall and its Passive Control Investigations on the OA209 Airfoil Section," *31st European Rotorcraft Forum*, National Aerospace Lab., Amsterdam, 13–16 Sept. 2005.

[22] Geissler, W., Dietz, G., Mai, H., Junker, B., and Lorkowski, T., "Dynamic Stall Control Investigations on a Full Size Chord Rotor Blade Section," *30th European Rotorcraft Forum*, National Aerospace Lab., Amsterdam, 14–16 Sept. 2004.

[23] Leschziner, M. A., and Drikakis, D., "Turbulence Modeling and Turbulent Flow Computation in Aeronautics," *The Aeronautical Journal*, Vol. 106, No. 1061, 2002, pp. 349–384.

[24] Spalart, P. R., and Allmaras, S. R., "A One Equation Turbulence Model for Aerodynamic Flows," AIAA Paper 92-0439, Jan. 1992.

[25] Michel, R., "Etude de la Transition sur le Profil d'Aile: Etablissement d'un Profil Incompressible," ONERA Rept. 1/1578A, Paris, 1951.

[26] Geissler, W., Chandrasekhara, M. S., Platzer, M., and Carr, L. W., "The Effect of Transition Modelling on the Prediction of Compressible Deep Dynamic Stall," *7th Asian Congress of Fluid Mechanics*, Asian Fluid Mechanics Com., 1997.